Nano Research
2022, 15(3): 2741–2745

ISSN 1998-0124 CN 11-5974/O4
https://doi.org/10.1007/s12274-021-3824-y

Research Article

Chiral self-assembly of terminal alkyne and selenium clusters organic–inorganic hybrid

Zhi Chen[1,2], Tao Lin[3], Haohan Li[2], Mingzi Sun[4], Chenliang Su[1] (✉), Bolong Huang[4] (✉), and Kian Ping Loh[2] (✉)

[1] *SZU-NUS Collaborative Innovation Center for Optoelectronic Science & Technology, International Collaborative Laboratory of 2D Materials for Optoelectronics Science and Technology of Ministry of Education, Institute of Microscale Optoelectronics, College of Chemistry and Environmental Engineering, Shenzhen University, Shenzhen 518060, China*

[2] *Department of Chemistry, Centre for Advanced 2D Materials (CA2DM), National University of Singapore, 3 Science Drive 3, Singapore 117543, Singapore*

[3] *College of New Materials and New Energies, Shenzhen Technology University, Shenzhen 518118, China*

[4] *Department of Applied Biology and Chemical Technology, The Hong Kong Polytechnic University, Hung Hom, Kowloon, Hong Kong SAR, China*

Received: 19 July 2021 / **Revised:** 15 August 2021 / **Accepted:** 16 August 2021

ABSTRACT

The on-surface self-assembly of inorganic atomic clusters and organic molecules offers significant opportunities to design novel hybrid materials with tailored functionalities. By adopting the advantages from both inorganic and organic components, the hybrid self-assembly molecules have shown great potential in future optoelectrical devices. Herein, we report the co-deposition of 4,8-diethynylbenzo[1,2-d-4,5-d0]bisoxazole (DEBBA) and Se atoms to produce a motif-adjustable organic–inorganic hybrid self-assembly system via the non-covalent interactions. By controlling the coverage of Se atoms, various chiral molecular networks containing Se, Se_6, Se_8, and terminal alkynes evolved on the Ag(111) surface. In particular, with the highest coverage of Se atoms, phase segregation into alternating one-dimensional chains of non-covalently bonded Se_8 clusters and organic ligands has been noticed. The atom-coverage dependent evolution of self-assembly structures reflects the remarkable structural adaptability of Se clusters as building blocks based on the spontaneous resize to reach the maximum non-covalent interactions. This work has significantly extended the possibilities of flexible control in self-assembly nanostructures to enable more potential functions for broad applications.

KEYWORDS

self-assembly, inorganic–organic hybrid, chiral, Se cluster, concentration-dependent

1 Introduction

Understanding how weak intermolecular interactions among molecular building blocks drive self-assembly systems allows us to design two-dimensional (2D) mesoscopic systems with new properties. On-surface Kagome lattice [1–8], tessellation [9, 10], pattern alloy [11], and even quasicrystals [12–17], and Sierpinski triangle fractals [18–22] have been discovered recently by using scanning tunneling microscopy (STM) and added to the list of artificially created low dimensional structures [23–26].

Among these on-surface self-assembies, chirality is an important research topic. STM provides the best model under atomic resolution to study 2D material structures, especially chiral self-assembly [24, 27, 28]. To construct 2D chiral self-assembly, one way is using chiral molecules [29]; another way is using achiral molecules to build a 2D chiral pattern with weak intermolecular interaction [1, 30, 31]; the third way is inducing guest molecules onto achiral self-assembly to form new surface structural chirality [8, 32]. Normally the guests are small organic molecules and very limited inorganic molecules. Other than the traditional organic self-assembly system, interests have turned to organic–inorganic hybrid materials [33–36]. Organic–inorganic hybrid materials such as hybrid perovskites [37–39] are one kind of important self-assembly through weak interactions such as hydrogen bonding, van der Waals forces, electrostatic interactions, or strong coordinative bonds. They have evolved into one of the most active research fields because they have the advances of organic materials with diversity, flexibility, and reproducibility, and also the advances of inorganic material of semiconducting, rigidity, and multifunction of metal centers.

However, it is uncommon for main group elements, in the form of atomic clusters with closed-shell electronic configuration, to be used as a building block in constructing an organic–inorganic hybrid system. One of the elemental building blocks of biological enzymes or proteins is sulfur and selenium. Selenium clusters like Se_6 [40] and Se_8 [41, 42] possess closed-shell electronic structures and thus are highly stable. Se clusters may interact via van der Waals interactions to form rectangular lattices on surfaces [43, 44]. However, the interaction of Se clusters with organic molecules to form the hybrid 2D self-assembly system has not been explored so far.

Herein, we report a chiral self-assembly system constructed of organic molecules and Se_6 or Se_8 clusters. Onto an achiral assembly of organic precursors 4,8-diethynylbenzo[1,2-d-4,5-d0]bisoxazole (DEBBA) on Ag(111), we dose Se atoms to

Address correspondence to Chenliang Su, chmsuc@szu.edu.cn; Bolong Huang, bhuang@polyu.edu.hk; Kian Ping Loh, chmlohkp@nus.edu.sg

investigate how Se atom partition itself among the organic molecules and form new hybrid phases. Depending on the coverage of Se atoms, three distinct chiral molecular networks consisting of sized-adjustable Se_n clusters (n = 1, 6, and 8) and DEBBA were formed. Our results show the remarkable structural flexibility of the hybrid organic–inorganic system in forming supramolecular structures as a function of the concentration of inorganic atoms.

2 Results and discussion

The precursor DEBBA was synthesized according to the methods described in our previous work [45]. After the deposition of DEBBA onto Ag(111) held at room temperature, the highly uniform chevron-type arrangement of DEBBA was obtained over a large area (Fig. 1(a)). The individual molecule of DEBBA shows a bicone-like protrusion. The monolayer pattern is mainly formed by C–H···O hydrogen-bonding between two adjacent DEBBA ligands (Fig. 1(b)). To simulate the STM images, we performed density functional theory (DFT) calculations of the self-assembled DEBBA structures on Ag(111) substrate. The relaxed DEBBA molecules maintain a flat structure with hydrogen bonding between the molecules. The DEBBA molecules maintain a distance of 3.41 Å from the Ag substrate, indicating a relatively weak interaction with the surface (Fig. 1(c)). The simulated STM image with an applied bias voltage of −1.0 V confirms that the two DEBBA orientations can be distinguished on the Ag(111) surface (Fig. 1(d)).

After the deposition of Se atoms onto the self-assembled network of DEBBA on Ag(111) at room temperature, a new phase named phase I, was formed (Fig. 2(a)). As shown in Fig. 2(c), a dumbbell-shape dimerd consisting of two DEBBA molecules at two ends and one Se atom in the middle is observed, which corresponds to a Se-to-DEBBA ratio of 1:2. The distance between the two centers of DEBBA is 1.32(5) nm (Fig. 2(d)), indicating that the terminal alkyne has lost one hydrogen atom to form an ethynyl selenide compound [46]. This dimer structure serves as the second type of building-block. The third-buildingblock comes from three dimers forming a triangle, which can adopt either a

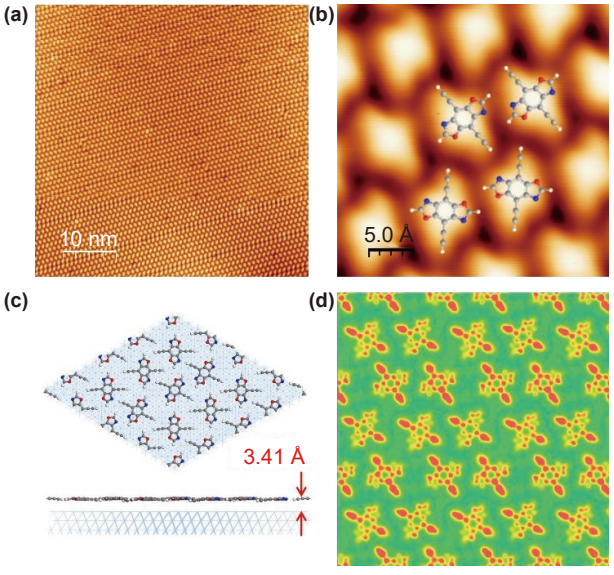

Figure 1 (a) STM image of self-assembly of DEBBA on Ag(111). (b) High-resolution STM image of the self-assembly of DEBBA superimposed with chemical models. (c) Top view and side view of the relaxed self-assembly of DEBBA after DFT calculations. (d) The simulated STM image with an applied bias voltage of −1.0 V. Scanning parameter for (a) and (b): U = −1.0 V and I = 0.1 nA.

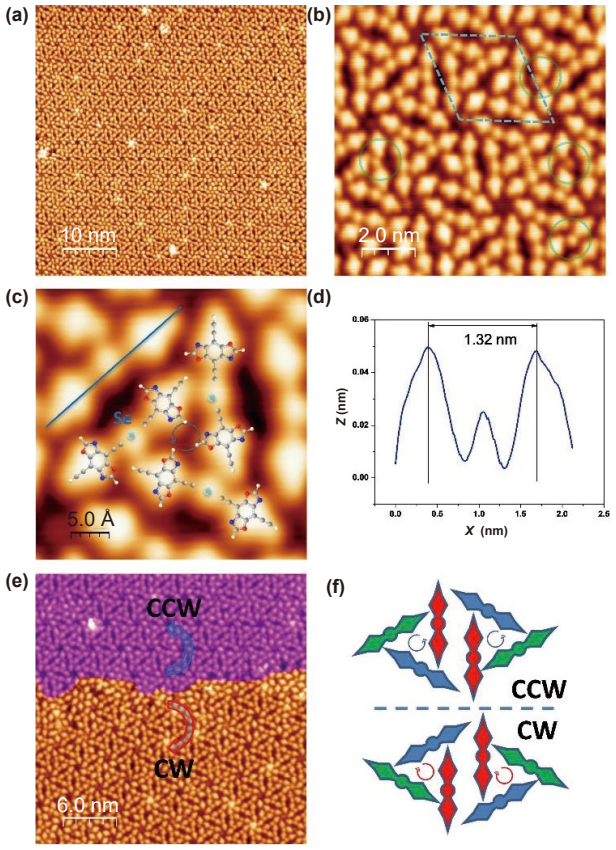

Figure 2 (a) Large-scale STM image of phase I (self-assembly of ethynyl selenide) on Ag(111). (b) and (c) High-resolution STM image of phase I superimposed with chemical models. (d) Height profile of blue line in (c). (e) CW and CCW domains of phase I. (f) Schematic illustration of the chirality. Scanning parameter for (a)–(c) and (e): U = −1.5 V and I = 0.1 nA.

clockwise (CW) or counter clockwise (CCW) (Figs. 2(c), 2(e), and 2(f)) orientation. The angle between two adjacent triangles is 60°, and six triangles can be oriented in either CCW or CW hexagonal pattern (Figs. 2(b) and 2(c)). This phase has a rhombus lattice with a unit cell length of 3.43(5) nm (Fig. 2(b)). The center of the hexagon forms a six-fold windmill by hydrogen bond of C–H···π electrons of alkyne terminals (Fig. 2(b)). Some defects (green circles in Fig. 2(b)) can also be found in the self-assembly; when the dumbbell-shaped structure is not formed, isolated Se atoms can be seen. This suggests that the middle atom in the dumbbell is not the Ag atom from the Ag(111) surface but Se single atom.

The self-assembled structure continually evolves when additional Se atoms are added. When the ratio of Se:DEBBA exceeds 1:1, the formation of the Se_6 ring influences the packing of DEBBA due to hydrogen bonding between H from DEBBA and the Se_6 ring, and a new phase is formed (phase II), as shown in Fig. 3(a). As shown in the high-resolution STM image and the corresponding chemical model (Fig. 3(b)), three different orientations of DEBBA molecules can be identified in the network (marked as red, blue, and green in Fig. 3(f), respectively). Six DEBBA molecules form a six-fold windmill shape with a CCW chirality. This windmill-shaped nanopore is bounded by C–H···π interaction of the hydrogen from the alkyne group and the nearby alkyne group. In the middle of the pore, the overlap of the in-plane π-orbitals among neighboring alkynes creates positively charged electronic states [30]. The positively charged hole acts as a host to the electron-rich Se_6 molecules, resulting in organic–inorganic self-assembly. In Fig. 3(b), the Se_6 cluster adopts a cyclohexane configuration with alternatingly high and low Se atoms, and three of the higher atoms manifest as a bright triangle protrusion occupying the hexagonal pore. There are also

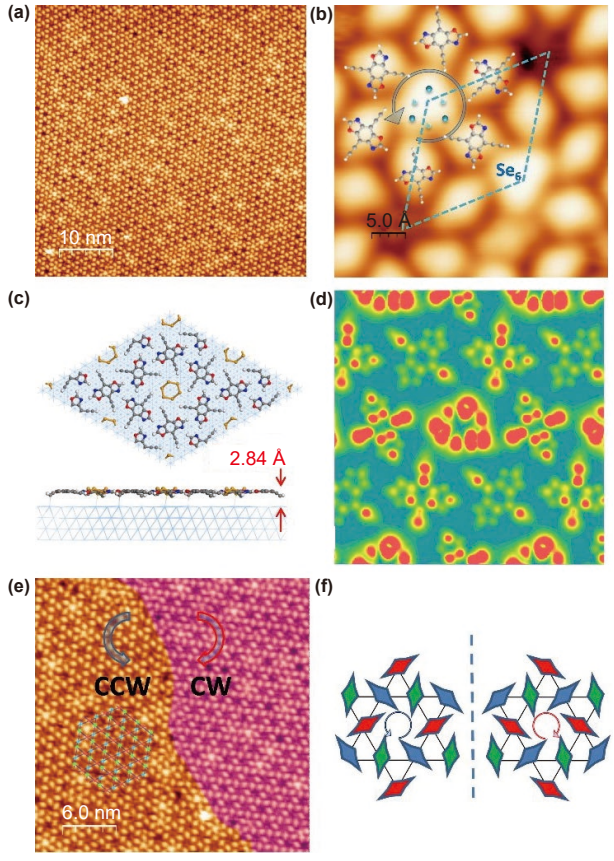

Figure 3 (a) Large-scale STM image of phase II (Kagome lattice of DEBBA with Se_6) on Ag(111). (b) High-resolution STM image of phase II superimposed with Kagome lattice symbol and chemical models. (c) Top view and side view of phase II on Ag(111) of DFT calculations. (d) The simulated STMs with an applied bias voltage of −1.0 V. (e) Coexisting CW and CCW phase II. (f) Schematic illustration of the Kagome-lattice chirality. Scanning parameter for (a), (b), and (e): $U = -1.0$ V and $I = 0.1$ nA.

some hexagonal pores that are not occupied by Se_6 structures and show a darker feature. Considering each DEBBA molecule as a node, the entire Se_6 cluster-organic molecules form a chiral Kagome geometry with CW or CCW chirality (Figs. 3(e) and 3(f)). This phase has a rhombus lattice with a unit cell length of 1.72(2) nm (Fig. 3(b)).

According to our DFT calculation, the Se_6 cluster adopts a chair conformation, in agreement with the experimental STM results showing the three-up and three-down triangle spots (Figs. 3(c) and 3(d)). The interlayer distance between the assembly layer and the Ag substrate has been reduced to 2.84 Å (Fig. 3(c)), indicating that the presence of Se clusters enhances the interaction with the substrate. From the DFT-calculated total density of states (TDOS) plot, the dominant peak of s, p orbitals from Se_6 is closer to the Fermi level (E_F) by 1.07 eV compared with the s, p orbitals from alkyne edges of the organic ligands (Fig. S1 in Electronic Supplementary Material (ESM)). The deeper-lying energy levels of the alkyne ligands are consistent with the electron-rich feature induced by the overlap between nearby π orbitals.

Further increasing the Se ratio to DEBBA (8:1) on Ag(111), the self-assembly structure now consists of alternating DEBBA and Se_8 chains (phase III) form (Fig. 4(a)). As shown in the high resolution STM image in Fig. 4(b), the Se_8 molecular cluster has a square shape. Four Se atoms at the square corners show protrusion feature, while the other four Se atoms at the middle of each side show depression feature. The dimension of these Se_8 clusters is 0.52(2) nm, which is similar to that reported for 0.53 nm for Se_8 rings [41–43, 47]. Different from the perfect boat conformation of Se_8 molecules in bulk crystals, such a square feature is probably due to the formation of weak Se–Ag bonds on the surface [43]. Adjacent Se_8 molecules are offset to form a zigzag line owing to the electrostatic repulsion.

With weak hydrogen bonding interactions of DEBBA molecules and Se_8 molecules, the DEBBA molecules also adopt a one-dimensional (1D) packing. As shown in Fig. 4(b), the 1D DEBBA structure shows a parallelogram unit cell with $a = 1.86(2)$ and $b = 0.92(2)$ nm and an angle of 70°. The zigzag aligned Se_8 and DEBBA structure as shown in Fig. 4(b) has also been confirmed by DFT calculations. The bright and dark contrast in the STM originates from the DEBBA and Se_8, respectively. The simulated STM image of the relaxed structure under a similar bias voltage of −1.5 V reproduces the squarish feature (Fig. 4(d)). Due to the zigzag packing of Se_8 molecules and the bicone-like shape of the DEBBA molecule, the total packing presents a left-hand or right-hand chirality (Figs. 4(e) and 4(f)). The thermal stability of these self-assembled structures is tested by annealing. After 100 °C annealing, some parts of phase III start to decompose (as shown in Fig. S2(a) in the ESM). Based on the zoom-in STM image of the decomposed phase III (Fig. S2(b) in the ESM), we can find that the Se atoms cluster and form a solid solution, and DEBBA molecules are scattered in the Se solution. After further annealing to 120 °C, both phases II and III are decomposed, but phase I remains intact. As shown in Fig. S2(c) in the ESM, there are mixed phases of I and II after annealing, whereby phase I remains intact, while phase II has been decomposed. This reveals that phase I is the most stable phase, due to the strong interactions between ethynyl groups and selenium atoms.

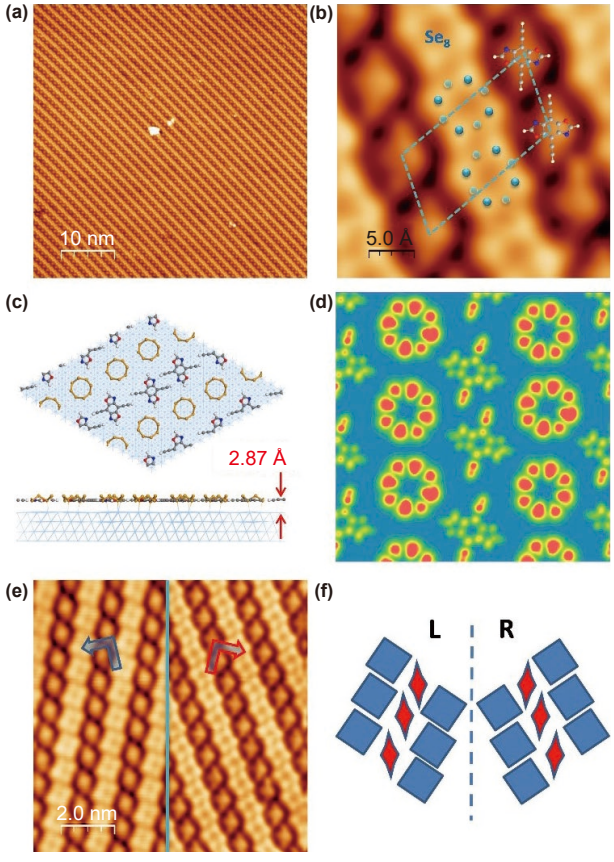

Figure 4 (a) Overview STM image of phase III (linear self-assembly of Se_8 and DEBBA). (b) High-resolution STM image of phase III superimposed with the chemical model. (c) Top view and side view of phase III on Ag(111) of DFT calculations. (d) The simulated STMs with an applied bias voltage of −1.50 V. (e) STM images of phase III exhibiting left-hand and right-hand chirality. (f) Schematic illustration of the chirality. Scanning parameter for (a), (b), and (e): $U = -1.5$ V, $I = 0.1$ nA.

Our study reveals the remarkable self-organization of selenium atoms with organic molecules. Depending on the number of coordinating and hydrogen bonds between the organic molecules and Se atoms, the complex self-organized mesoscopic structure can be formed. It is well known that Se atoms can undergo aggregation, and thus Se, Se_6, Se_8, Se_{12}, and even 1D Se can be observed on Ag(111) (Fig. S3 in the ESM). At the boundaries between the two self-organised phases, Se_1, Se_6, Se_8, and Se_{12} species can be observed (Fig. S3(a) in the ESM). At the initial stage of the self-assembly of the organic and inorganic components, Se_1, Se_6, Se_8, and Se_{12} species can also be found among the 1D polymer of DEBBA (Fig. S3(c) in the ESM). However, in the absence of organic ligands terminating the edges, these aggregates typically form a hexagonal phase (Fig. S3(d) in the ESM) when the surface concentration of Se atoms increases. By contrast, the presence of organic ligands stabilizes the Se_8 1D self-assembly to form a chiral 2D self-assembly. Among the self-assembly structure, the most striking is phase III, which can be considered as a 1D assembly of alternating organic and inorganic moieties, bonded at the edges by non-covalent interactions. It would be interesting to study the catalytic properties of these self-assembly Se clusters supported on metallic substrate separated by the organic molecular system for reactions that occur at room temperature. The study may be extended to other metallic clusters, the literature has abundant reports on metal clusters that are stabilized by organic ligands in solution, what we discovered here is that a 2D or 1D periodic motif of these can be extended to surfaces. Interestingly, the chirality of these self-assembly phases I to III of DEBBA molecules and Se species belongs to a kind of chirality, which is created by inducing achiral guest molecules onto achiral self-assembly [8, 32]. After deposition of Se to the self-assembly of DEBBA, more kinds of weak interactions are induced, helping the formation of chiral self-assembly. Our research enriches this kind of surface chiral species case.

3 Conclusions

In summary, we have developed hybrid organic–inorganic 2D materials through the precise control of self-assembly 2D materials. By controlling the coverage of Se atoms, various chiral molecular networks containing Se, Se_6, Se_8, and terminal alkynes DEBBA can be formed on Ag(111). The concentration of Se atoms is the key to the modulations of Se cluster types. At low coverage of Se atoms, the Se atom and two DEBBA molecules form a dumbbell dimer ethynyl selenide and further form a chiral complex pattern; at middle coverage of Se atoms, the self-assembly structure is made of Se_6 clusters occupying the pore sites of the chiral Kagome lattice of organic self-assembly framework; at high coverage of Se atoms, the structure phase segregates into alternating one-dimensional chains of non-covalently bonded Se_8 clusters and organic ligands. This research has supplied significant references to the hybrid organic–inorganic 2D material design, which further expands the applications of on-surface self-assembly in fabricating novel materials.

Acknowledgements

This work was supported by the Guangdong Basic and Applied Basic Research Foundation (Nos. 2019A1515110819 and 2020A1515010767), NRF-CRP grant "Two Dimensional Covalent Organic Framework: Synthesis and Applications" (No. NRF-CRP16-2015-02, funded by National Research Foundation, Prime Minister's Office, Singapore), the Shenzhen Peacock Plan (No. KQTD2016053112042971), and the National Natural Science Foundation of China (Nos. 21802067 and 21771156).

Electronic Supplementary Material: Supplementary material (further details of the sample preparation procedures, STM measurements, and theoretical calculations) is available in the online version of this article at https://doi.org/10.1007/s12274-021-3824-y.

References

[1] Schlickum, U.; Decker, R.; Klappenberger, F.; Zoppellaro, G.; Klyatskaya, S.; Auwärter, W.; Neppl, S.; Kern, K.; Brune, H.; Ruben, M. et al. Chiral kagomé lattice from simple ditopic molecular bricks. *J. Am. Chem. Soc.* **2008**, *130*, 11778–11782.

[2] Shi, Z. L.; Lin, N. Porphyrin-based two-dimensional coordination Kagome lattice self-assembled on a Au(111) surface. *J. Am. Chem. Soc.* **2009**, *131*, 5376–5377.

[3] Chen, T.; Chen, Q.; Zhang, X.; Wang, D.; Wan, L. J. Chiral Kagome network from thiacalix[4]arene tetrasulfonate at the interface of aqueous solution/Au(111) surface: An *in situ* electrochemical scanning tunneling microscopy study. *J. Am. Chem. Soc.* **2010**, *132*, 5598–5599.

[4] Chen, Q.; Bae, S. C.; Granick, S. Directed self-assembly of a colloidal kagome lattice. *Nature* **2011**, *469*, 381–384.

[5] Wang, T.; Fan, Q. T.; Feng, L.; Tao, Z. J.; Huang, J. M.; Ju, H. X.; Xu, Q.; Hu, S. W.; Zhu, J. F. Chiral Kagome lattices from on-surface synthesized molecules. *ChemPhysChem* **2017**, *18*, 3329–3333.

[6] Xing, L. B.; Jiang, W.; Huang, Z. C.; Liu, J.; Song, H. J.; Zhao, W. H.; Dai, J. X.; Zhu, H.; Wang, Z. H.; Weiss, P. S. et al. Steering two-dimensional porous networks with σ-hole interactions of Br···S and Br···Br. *Chem. Mater.* **2019**, *31*, 3041–3048.

[7] Hernández-López, L.; Piquero-Zulaica, I.; Downing, C. A.; Piantek, M.; Fujii, J.; Serrate, D.; Ortega, J. E.; Bartolomé, F.; Lobo-Checa, J. Searching for kagome multi-bands and edge states in a predicted organic topological insulator. *Nanoscale* **2021**, *13*, 5216–5223.

[8] Adisoejoso, J.; Tahara, K.; Okuhata, S.; Lei, S. B.; Tobe, Y.; De Feyter, S. Two-dimensional crystal engineering: A four-component architecture at a liquid–solid interface. *Angew. Chem., Int. Ed.* **2009**, *48*, 7353–7357.

[9] Écija, D.; Urgel, J. I.; Papageorgiou, A. C.; Joshi, S.; Auwärter, W.; Seitsonen, A. P.; Klyatskaya, S.; Ruben, M.; Fischer, S.; Vijayaraghavan, S. et al. Five-vertex Archimedean surface tessellation by lanthanide-directed molecular self-assembly. *Proc. Natl. Acad. Sci. USA.* **2013**, *110*, 6678–6681.

[10] Zhang, Y. Q.; Paszkiewicz, M.; Du, P.; Zhang, L. D.; Lin, T.; Chen, Z.; Klyatskaya, S.; Ruben, M.; Seitsonen, A. P.; Barth, J. V. et al. Complex supramolecular interfacial tessellation through convergent multi-step reaction of a dissymmetric simple organic precursor. *Nat. Chem.* **2018**, *10*, 296–304.

[11] Cheng, F.; Wu, X. J.; Hu, Z. X.; Lu, X. F.; Ding, Z. J.; Shao, Y.; Xu, H.; Ji, W.; Wu, J. S.; Loh, K. P. Two-dimensional tessellation by molecular tiles constructed from halogen–halogen and halogen–metal networks. *Nat. Commun.* **2018**, *9*, 4871.

[12] Sharma, H. R.; Nozawa, K.; Smerdon, J. A.; Nugent, P. J.; McLeod, I.; Dhanak, V. R.; Shimoda, M.; Ishii, Y.; Tsai, A. P.; McGrath, R. Templated three-dimensional growth of quasicrystalline lead. *Nat. Commun.* **2013**, *4*, 2715.

[13] Wasio, N. A.; Quardokus, R. C.; Forrest, R. P.; Lent, C. S.; Corcelli, S. A.; Christie, J. A.; Henderson, K. W.; Kandel, S. A. Self-assembly of hydrogen-bonded two-dimensional quasicrystals. *Nature* **2014**, *507*, 86–89.

[14] Urgel, J. I.; Écija, D.; Lyu, G. Q.; Zhang, R.; Palma, C. A.; Auwärter, W.; Lin, N.; Barth, J. V. Quasicrystallinity expressed in two-dimensional coordination networks. *Nat. Chem.* **2016**, *8*, 657–662.

[15] Collins, L. C.; Witte, T. G.; Silverman, R.; Green, D. B.; Gomes, K. K. Imaging quasiperiodic electronic states in a synthetic Penrose tiling. *Nat. Commun.* **2017**, *8*, 15961.

[16] Kalashnyk, N.; Ledieu, J.; Gaudry, É.; Cui, C.; Tsai, A. P.; Fournée, V. Building 2D quasicrystals from 5-fold symmetric corannulene molecules. *Nano Res.* **2018**, *11*, 2129–2138.

[17] Paßens, M.; Karthäuser, S. Rotational switches in the two-

dimensional fullerene quasicrystal. *Acta Crystallogr. A:Found Adv.* **2019**, *75*, 41–49.
[18] Shang, J.; Wang, Y. F.; Chen, M.; Dai, J. X.; Zhou, X.; Kuttner, J.; Hilt, G.; Shao, X.; Gottfried, J. M.; Wu, K. Assembling molecular Sierpiński triangle fractals. *Nat. Chem.* **2015**, *7*, 389–393.
[19] Li, N.; Zhang, X.; Gu, G. C.; Wang, H.; Nieckarz, D.; Szabelski, P.; He, Y.; Wang, Y.; Lü, J. T.; Tang, H. et al. Sierpiński-triangle fractal crystals with the C_{3v} point group. *Chin. Chem. Lett.* **2015**, *26*, 1198–1202.
[20] Mo, Y. P.; Chen, T.; Dai, J. X.; Wu, K.; Wang, D. On-surface synthesis of highly ordered covalent Sierpiński triangle fractals. *J. Am. Chem. Soc.* **2019**, *141*, 11378–11382.
[21] Wang, Y. F.; Xue, N.; Li, R. N.; Wu, T. H.; Li, N.; Hou, S. M.; Wang, Y. F. Construction and properties of Sierpinski triangular fractals on surfaces. *ChemPhysChem* **2019**, *20*, 2262–2270.
[22] Feng, G. Y.; Shen, Y. T.; Yu, Y. X.; Liang, Q.; Dong, J.; Lei, S. B.; Hu, W. P. Boronic ester Sierpinski triangle fractals: From precursor design to on-surface synthesis and self-assembling superstructures. *Chem. Commun.* **2021**, *57*, 2065–2068.
[23] Elemans, J. A. A. W.; Lei, S. B.; De Feyter, S. Molecular and supramolecular networks on surfaces: From two-dimensional crystal engineering to reactivity. *Angew. Chem., Int. Ed.* **2009**, *48*, 7298–7332.
[24] Chen, T.; Wang, D.; Wan, L. J. Two-dimensional chiral molecular assembly on solid surfaces: Formation and regulation. *Natl. Sci. Rev.* **2015**, *2*, 205–216.
[25] Mali, K. S.; Pearce, N.; De Feyter, S.; Champness, N. R. Frontiers of supramolecular chemistry at solid surfaces. *Chem. Soc. Rev.* **2017**, *46*, 2520–2542.
[26] Xing, L. B.; Peng, Z. T.; Li, W. T.; Wu, K. On controllability and applicability of surface molecular self-assemblies. *Acc. Chem. Res.* **2019**, *52*, 1048–1058.
[27] Huan, J. W.; Zhang, X. M.; Zeng, Q. D. Two-dimensional supramolecular crystal engineering: Chirality manipulation. *Phys. Chem. Chem. Phys.* **2019**, *21*, 11537–11553.
[28] Li Y. H.; Yu C. B.; Li Z.; Jiang, P. Zhou, X. Y.; Gao C. F.; Li J. Y. Layer-dependent and light-tunable surface potential of two-dimensional indium selenide (InSe) flakes. *Rare Met.* **2020**, *39*, 1356–1363.
[29] Zaera, F. Chirality in adsorption on solid surfaces. *Chem. Soc. Rev.* **2017**, *46*, 7374–7398.
[30] Zhang, Y. Q.; Björk, J.; Barth, J. V.; Klappenberger, F. Intermolecular hybridization creating nanopore orbital in a supramolecular hydrocarbon sheet. *Nano Lett.* **2016**, *16*, 4274–4281.
[31] Chen, Q.; Chen, T.; Wang, D.; Liu, H. B.; Li, Y. L.; Wan, L. J. Structure and structural transition of chiral domains in oligo(p-phenylenevinylene) assembly investigated by scanning tunneling microscopy. *Proc. Natl. Acad. Sci. USA.* **2010**, *107*, 2769–2774.
[32] Liu, J.; Chen, T.; Deng, X.; Wang, D.; Pei, J.; Wan, L. J. Chiral hierarchical molecular nanostructures on two-dimensional surface by controllable trinary self-assembly. *J. Am. Chem. Soc.* **2011**, *133*, 21010–21015.
[33] Hu, B. J.; Wu, P. Y. Facile synthesis of large-area ultrathin two-dimensional supramolecular nanosheets in water. *Nano Res.* **2020**, *13*, 868–874.
[34] Fang, Z. W.; Xing, Q. Y.; Fernandez, D.; Zhang, X.; Yu, G. H. A mini review on two-dimensional nanomaterial assembly. *Nano Res.* **2020**, *13*, 1179–1190.
[35] Yuan, Z.; Tai, H. L.; Su, Y. J.; Xie, G. Z.; Du, X. S.; Jiang, Y. D. Self-assembled graphene oxide/polyethyleneimine films as high-performance quartz crystal microbalance humidity sensors. *Rare Met.* **2021**, *40*, 1597–1603.
[36] Huang, M.; Liu, J. X.; Huang, P.; Hu, H.; Lai, C. Self-assembly synthesis of $SnNb_2O_6$/amino-functionalized graphene nanocomposite as high-rate anode materials for sodium-ion batteries. *Rare Met.* **2021**, *40*, 425–432.
[37] Lyu, M. Q.; Yun, J. H.; Cai, M. L.; Jiao, Y. L.; Bernhardt, P. V.; Zhang, M.; Wang, Q.; Du, A. J.; Wang, H. X.; Liu, G.; et al. Organic–inorganic bismuth (III)-based material: A lead-free, air-stable and solution-processable light–absorber beyond organolead perovskites. *Nano Res.* **2016**, *9*, 692–702.
[38] Brenner, T. M.; Egger, D. A.; Kronik, L.; Hodes, G.; Cahen, D. Hybrid organic–inorganic perovskites: Low-cost semiconductors with intriguing charge-transport properties. *Nat. Rev. Mater.* **2016**, *1*, 15007.
[39] Saparov, B.; Mitzi, D. B. Organic–inorganic perovskites: Structural versatility for functional materials design. *Chem. Rev.* **2016**, *116*, 4558–4596.
[40] Dietz, J.; Müller, U.; Müller, V.; Dehnicke, K. The crystal structures of $(NEt_4^+)_2[Se_5^{2-} \cdot 1/2\ Se_6 \cdot Se_7]$ and $(NPr_4)_2Se_{11}$. *Z. Naturforsch. B* **1991**, *46*, 1293–1299.
[41] Panthöfer, M.; Shopova, D.; Jansen, M. Crystal structure and stablility of the fullerene–chalcogene co-crystal $C_{60}Se_8CS_2$. *Z. Anorg. Allg. Chem.* **2005**, *631*, 1387–1390.
[42] Shopova, D.; Panthöfer, M.; Petricek, V.; Jansen, M. Refinement strategies for fullerene structures: Use of local, non-crystallographical point group symmetry. *Z. Kristallogr.* **2007**, *222*, 546–550.
[43] Lister, T. E.; Stickney, J. L. Atomic level studies of selenium electrodeposition on Gold(111) and Gold(110). *J. Phys. Chem.* **1996**, *100*, 19568–19576.
[44] Ruano, G.; Tosi, E.; Sanchez, E.; Abufager, P.; Martiarena, M. L.; Grizzi, O.; Zampieri, G. Stages of Se adsorption on Au(111): A combined XPS, LEED, TOF-DRS, and DFT study. *Surf. Sci.* **2017**, *662*, 113–122.
[45] Chen, Z.; Lin, T.; Li, H. H.; Cheng, F.; Su, C. L.; Loh, K. P. Hydrogen bond guided synthesis of close-packed one-dimensional graphdiyne on the Ag(111) surface. *Chem. Sci.* **2019**, *10*, 10849–10852.
[46] Wang, D. L.; Fang, Y.; Wang, S. Y.; Ji, S. J. Silver-mediated activation of terminal alkynes: A strategy to construct bis-ethynyl selenides and tellurides. *Tetrahedron* **2020**, *76*, 131083.
[47] Karhu, A. J.; Pakkanen, O. J.; Rautiainen, J. M.; Oilunkaniemi, R.; Chivers, T.; Laitinen, R. S. Experimental and computational ^{77}Se NMR investigations of the cyclic eight-membered selenium imides 1, 3, 5, 7-$Se_4(NR)_4$ (R = Me, ^{t}Bu) and 1, 5-$Se_6(NMe)_2$. *Inorg. Chem.* **2015**, *54*, 4990–4997.